Edge-Mode Lasing in 1D Topological Active Arrays

Midya Parto,[1] Steffen Wittek,[1] Hossein Hodaei,[1] Gal Harari,[2] Miguel A. Bandres,[2] Jinhan Ren,[1] Mikael C. Rechtsman,[3] Mordechai Segev,[2] Demetrios N. Christodoulides,[1,*] and Mercedeh Khajavikhan[1,†]

[1]*CREOL/College of Optics and Photonics, University of Central Florida, Orlando, Florida 32816, USA*

[2]*Department of Physics, Technion-Israel Institute of Technology, Haifa 32000, Israel*

[3]*Department of Physics, The Pennsylvania State University, University Park, Pennsylvania 16802-6300, USA*

(Received 19 July 2017; revised manuscript received 18 September 2017; published 15 March 2018)

We report the first observation of lasing topological edge states in a 1D Su-Schrieffer-Heeger active array of microring resonators. We show that the judicious use of non-Hermiticity can promote single edge-mode lasing in such arrays. Our experimental and theoretical results demonstrate that, in the presence of chiral-time symmetry, this non-Hermitian topological structure can experience phase transitions that are dictated by a complex geometric phase. Our work may pave the way towards understanding the fundamental aspects associated with the interplay among non-Hermiticity, nonlinearity, and topology in active systems.

DOI: 10.1103/PhysRevLett.120.113901

In condensed matter physics, topological insulators (TIs) represent new forms of matter wherein electron conduction is prohibited in the bulk, while it is allowed along the surface by means of edge states [1–4]. These gapless edge states emerge whenever a TI either is terminated on a vacuum or is interfaced with an ordinary insulator—a principle known as bulk-edge correspondence. Consequently, topological edge states are robust against local perturbations, since their characteristics are dictated by their corresponding bulk environment. This is in sharp contrast to conventional defect states that originate from imperfections and are by nature sensitive to perturbations. It is this robustness that has incited a flurry of activities aimed to understand and harness the ramifications of topology in many and diverse fields [5–17]. In optics, the newly emerging field of topological photonics aims to fundamentally explore and technologically utilize the effect of topological protection in order to demonstrate novel devices and functionalities. As indicated in recent studies, the introduction of topology in photonics can lead to a host of intriguing and unexpected results. These include unidirectional light transport and backscattered-free light propagation as well as immunity to structural imperfections [6]. In photonics, the availability of gain and loss (non-Hermiticity) and the possibility of utilizing optical nonlinearities [18–26]—a set of attributes not present in solid-state materials—can provide even richer ground for topological physics. In this respect, one may ask a number of fundamental questions. For example, can a system lase in a topological edge mode, and what dictates the characteristics of such a laser? Can nonlinearity and non-Hermiticity impede or assist lasing topological edge states, and in that case how do topological attributes depend on the gain or loss levels?

In this Letter, we theoretically and experimentally investigate the lasing properties of Su-Schrieffer-Heeger (SSH) active microring resonator arrays. Such arrays present an archetypical example of one-dimensional discrete lattices that are known to be topologically nontrivial [27]. Thus far, this class of SSH structures has been employed to experimentally probe topological phase transitions [28,29] and to demonstrate $\mathcal{PT}$-symmetric topologically protected bound states in passive systems such as fused silica coupled waveguide arrays [30]. On the contrary, the optical SSH structures considered in this study are both nonlinear and highly non-Hermitian. We demonstrate that the conventional chiral $\mathcal{C}$ symmetry associated with the passive SSH system no longer persists in the presence of non-Hermiticity. Instead, by judiciously engineering the gain and loss profile in the SSH laser array in a way that respects $\mathcal{PT}$ symmetry, the ensuing Hamiltonian now possesses $\mathcal{CT}$ symmetry, a necessary ingredient in this case for robust topologically protected lasing edge states. Our analysis reveals three different phases that depend on the gain levels involved and the coupling strengths. We find that this rich nonlinear and non-Hermitian system displays a broad range of behaviors, starting from single edge-mode lasing and eventually ending in multimode emission within the bulk of the array. The observed intensity mode profiles and spectra emitted by this topological laser arrangement are in good agreement with theoretical predictions that account for carrier dynamics, saturable gain, and laser mode competition.

For our study, we fabricate an active SSH array consisting of 16 identical coupled microring resonators fabricated on InGaAsP quantum wells. The gain medium consists of six vertically stacked quantum wells, each composed of a 10-nm-thick well ($In_{x=0.56}Ga_{1-x}As_{y=0.93}P_{1-y}$) sandwiched between two 20-nm-thick barrier layers ($In_{x=0.74}Ga_{1-x}As_{y=0.57}P_{1-y}$), with an overall height of 200 nm, which is capped with a 10-nm-thick layer of InP,

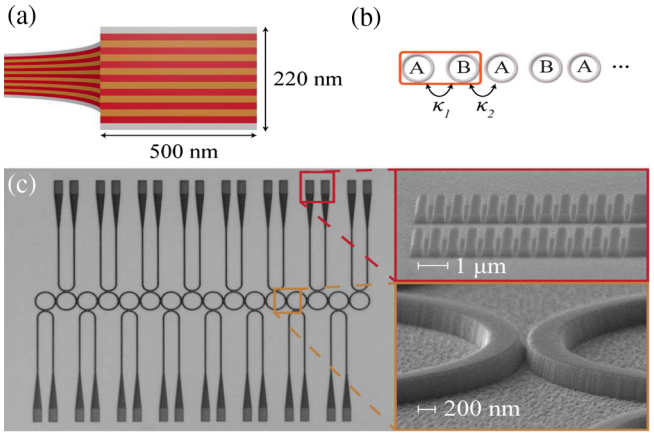

FIG. 1. (a) InGaAsP multilayer quantum well structure used in the microrings, (b) a schematic of the SSH microring laser array, and (c) a microscope image of the fabricated structure with 16 elements. The insets show scanning electron microscope images of the grating at the end of the outcoupling waveguides and the coupling region between two microrings.

as depicted in Fig. 1(a). The coupling strengths in this SSH structure alternate between $\kappa_1 \approx 8 \times 10^{10}\ \mathrm{s}^{-1}$ and $\kappa_2 \approx 14 \times 10^{10}\ \mathrm{s}^{-1}$, as obtained when the distance between successive rings is 200 and 150 nm, respectively. The resulting lattice shown in Fig. 1(b) involves a nontrivial termination, capable of supporting edge modes. Figure 1(c) shows a microscope image of a fabricated SSH structure (eight unit cells), with each ring being weakly coupled to a waveguide that happens to be equipped with two outcoupling gratings—necessary to interrogate the array. Within the tight-binding formalism, the dynamics in this SSH configuration can be described by the following Hamiltonian:

$$H_0 = \epsilon_A \sum_n \hat{c}_n^{A\dagger} \hat{c}_n^A + \epsilon_B \sum_n \hat{c}_n^{B\dagger} \hat{c}_n^B + \sum_n [\kappa_1 (\hat{c}_n^{B\dagger} \hat{c}_n^A + \hat{c}_n^{A\dagger} \hat{c}_n^B) + \kappa_2 (\hat{c}_{n-1}^{B\dagger} \hat{c}_n^A + \hat{c}_n^{A\dagger} \hat{c}_{n-1}^B)], \tag{1}$$

where $\hat{c}_n^{A\dagger}$ and $\hat{c}_n^{B\dagger}$ denote photon creation operators at site n in the sublattices A and B of this structure, respectively, while ϵ_A and ϵ_B represent the complex on-site eigenfrequencies (potentials) of the corresponding active rings. Again, κ_1 and κ_2 are the intracell and intercell coupling coefficients, respectively. In momentum space representation, the Bloch mode Hamiltonian can be obtained through a Fourier transform, i.e.,

$$H_0(k) = \begin{pmatrix} \epsilon_A & \kappa_1 + \kappa_2 e^{-ik} \\ \kappa_1 + \kappa_2 e^{ik} & \epsilon_B \end{pmatrix}. \tag{2}$$

If the array is Hermitian and is composed of identical rings ($\epsilon_A = \epsilon_B = 0$), the Hamiltonian of Eq. (2) anticommutes with the chiral operator $\mathcal{C} = \sigma_z$. Because of the chiral symmetry, the eigenvalues are symmetrically distributed around zero, with the two zero-energy edge states being located at the ends of the Brillouin zone $k = \pm\pi$ [Fig. 2(a)]. The field of the edge modes exponentially decays into the bulk [see Fig. 2(a)]. Note that the field distribution of these edge modes is π staggered on the sublattices A and B. On the other hand, if the SSH structure is active, then the on-site potentials are now purely imaginary, i.e., $\epsilon_A = -ig_A$ and $\epsilon_B = -ig_B$. In this latter case, it is easy to show that the structure no longer possesses $\mathcal{C}$ symmetry, i.e., $\mathcal{C}H_0\mathcal{C}^{-1} \neq -H_0$. In our experimental realization [Fig. 1(b)], the parameters g_A and g_B are dictated by the linear gain coefficients associated with the two sublattices A and B, as induced by differential pumping. In general, the dynamics of such an active SSH lattice are described by [31,32]

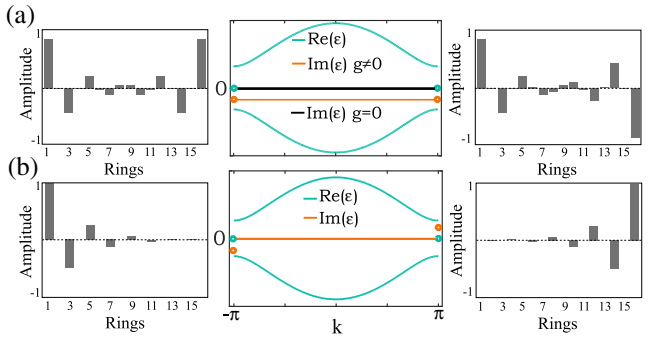

FIG. 2. Eigenvalue diagrams of an infinite (a) Hermitian and uniformly pumped ($g = 0$ and $g \neq 0$) and (b) $\mathcal{PT}$-symmetric SSH lattice, where the eigenvalues of the edge modes corresponding to a finite, nontrivial termination of the structure are also represented by dots at both ends of the Brillouin zone. The field profiles of the edge states are also depicted in the right and left insets.

$$\frac{dE_n^{A,B}}{dt} = \frac{1}{2}[-\gamma + \sigma(N_n^{A,B} - 1)](1 - i\alpha_H)E_n^{A,B} + i\kappa_1 E_n^{B,A} + i\kappa_2 E_{n\mp1}^{B,A},$$
$$\frac{dN_n^{A,B}}{dt} = R_{A,B} - N_n^{A,B}/\tau_r - F(N_n^{A,B} - 1)|E_n^{A,B}|^2. \tag{3}$$

Here, E_n^A and E_n^B denote the electric modal field amplitudes in sublattices A and B, respectively, γ is inversely proportional to the photon lifetime in each microring cavity, and N_n^A and N_n^B represent the carrier population densities normalized with respect to the transparency value N_0. In addition, α_H is the linewidth enhancement factor, $\sigma = \Gamma v_g a N_0$ is proportional to the unsaturated loss in the absence of pumping, Γ is the confinement factor, a is the gain proportionality factor, and $v_g = c/n_g$ denotes the group velocity within the cavity. The rest of the variables appearing in Eqs. (3) are defined in Ref. [33].

We first consider the simplest possible case, i.e., when the pumping is uniform $g_A = g_B = g$. The linear band structure of this SSH laser system under this condition is

also depicted in Fig. 2(a). The optical field distributions corresponding to the two edge states are identical to those in the Hermitian case. It is evident that, in this scenario, the eigenvalues are no longer symmetrically distributed around the zero level; instead, they all shift by the same amount $-ig$ (in their imaginary part), corresponding to an equal amount of gain g for all supermodes involved [red line in the dispersion curve in Fig. 2(a)]. This situation drastically changes once $\mathcal{PT}$ symmetry is introduced, i.e., $g_A = -g_B = g$. In this regime, the Hamiltonian of Eq. (2) now takes the form

$$H_0(k) = \begin{pmatrix} -ig & \rho \\ \rho^* & +ig \end{pmatrix}, \tag{4}$$

where $\rho = \kappa_1 + \kappa_2 e^{-ik}$. As previously indicated, this Hamiltonian does not respect the chiral $\mathcal{C}$ symmetry. Instead, H_0 satisfies

$$\mathcal{CT}_{PS} H_0 \mathcal{T}_{PS}^{-1} \mathcal{C}^{-1} = H_0, \tag{5}$$

where the pseudospin time reversal operator $\mathcal{T}_{PS}$ is here defined as $\mathcal{T}_{PS} = i\sigma_y \mathcal{K}$, with $\mathcal{K}$ denoting complex conjugation. If $|\psi\rangle$ is an eigenstate of H_0 ($H_0|\psi\rangle = \epsilon|\psi\rangle$), then $\mathcal{CT}_{PS}|\psi\rangle$ is also an eigenstate of H_0, with eigenvalue ϵ^*. While $\mathcal{PT}$ symmetry is imposed in real space, the $\mathcal{CT}$ operator acts in the momentum domain. Figure 2(b) shows the eigenvalues of this $\mathcal{CT}$-symmetric Hamiltonian when $g < |\kappa_2 - \kappa_1|$. The right and left sides of this figure display the field amplitudes of the edge states corresponding to the two imaginary eigenvalues marked in the plot (red dots at the edges of the dispersion diagrams). Evidently, the field distributions of these states occupy only one of the sublattices (A or B) and alternate in sign. As a result, one of these modes is expected to experience gain, while the other one an equal amount of loss. Note that, under $\mathcal{PT}$-symmetric conditions, all the bulk modes remain neutral (neither gain nor loss).

Figure 3(a) shows the steady-state intensity distribution as obtained from simulations [Eqs. (3)], for a 16-element SSH laser system when uniformly pumped at $R_{A,B} = 1.06/\tau_r$. In these simulations, we assume that $\alpha_H = 4$, $\tau_r = 4$ ns, and $\sigma = 6 \times 10^{11}$ s^{-1}. The dimerization $\nu = \kappa_2/\kappa_1$ for this array is $\nu = 2$. The resulting lasing profile is a complex mixture of all the supermodes (including the edge states) supported in this laser array. This is because all modes experience the same gain. Nevertheless, the emission wavelength in the array greatly depends on the site number [Fig. 3(c)]. Our theoretical analysis suggests that, in a large array, the edge state will lase at the resonance frequency of each ring (ω_0). In other words, the normalized frequency shift for the edge mode is zero ($\Omega/\kappa_1 = 0$). This is because the real part of the eigenvalue of the edge mode remains the same if the array is uniformly pumped. Conversely, the spectrum emanating from rings in the bulk

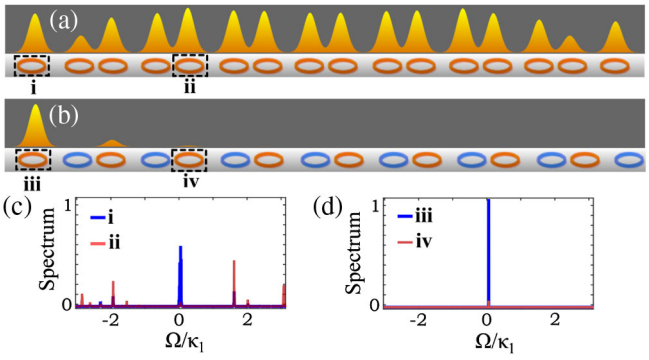

FIG. 3. Theoretically predicted steady-state lasing profiles for (a) uniformly pumped and (b) $\mathcal{PT}$-symmetric SSH lattice. Panels (c) and (d) depict the power spectra corresponding to the edge mode and bulk modes as obtained from different locations in the array.

(bulk modes) will have a considerably more complex structure because of mode competition effects. On the other hand, Fig. 3(b) shows the expected intensity distribution under $\mathcal{PT}$-symmetric conditions after numerically solving Eqs. (3)—starting from noise. In this case, the two sections are pumped at $R_A = 1.06/\tau_r$ while $R_B = 1.03/\tau_r$, thus setting sublattice A above lasing threshold, whereas B is kept below threshold. In this regime, our simulations show that only one of the edge modes (the one enjoying gain) is favored and hence lases, while all the bulk modes are suppressed. In direct contrast to the results presented in Fig. 3(a), $\mathcal{PT}$ symmetry now promotes only one edge state. Consequently, the spectrum emitted from the structure happens to be close to the ring resonance ω_0 and is single moded [Fig. 3(d)].

The dynamics of this $\mathcal{PT}$-symmetric SSH laser system can be theoretically predicted by considering the linear complex band structure associated with the non-Hermitian Hamiltonian of Eq. (4), which is given by

$$\epsilon(k) = \pm\kappa_1 \sqrt{1 + \nu^2 + 2\nu\cos(k) - \eta^2}, \tag{6}$$

where $\eta = g/\kappa_1$ represents a normalized gain or loss. This equation reveals three distinct phases, presented in Figs. 4(a)–4(c). If the SSH system is pumped or operated in the range of $0 < \eta < \nu - 1$ (denoted as phase I), only one edge state is expected to lase in a stable manner. In this domain, under steady-state conditions, the structure is single moded and the intensity profile across the array varies exponentially with the site number [inset in Fig. 4(a)]. As the gain in the topological system increases, i.e., when $\nu - 1 < \eta < \nu + 1$, the SSH structure enters phase II, where some of the bulk modes start to acquire complex eigenvalues (after entering the $\mathcal{PT}$-symmetry broken phase), resulting in a multimode operation [inset in Fig. 4(b)]. Note that in phase II the intensity profile across the array is asymmetrically one sided, biased

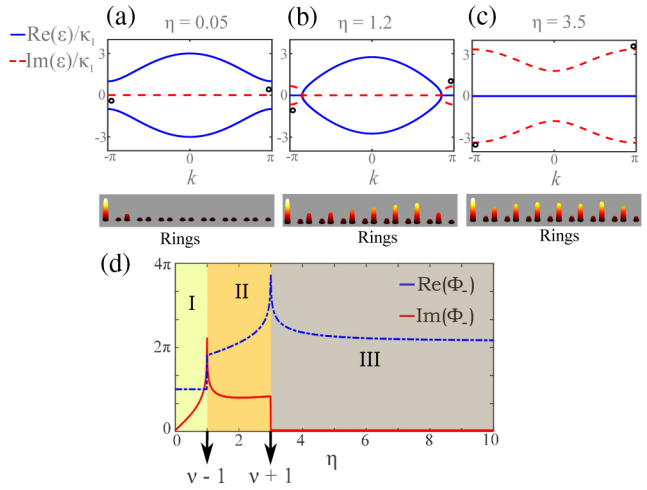

FIG. 4. Complex band structure of the infinite $\mathcal{PT}$-symmetric SSH model, where (a), (b), and (c) correspond to the three phases I, II, and III, respectively (the eigenvalues of the edge modes corresponding to a finite, nontrivial termination of the structure are depicted by dots at both ends of the Brillouin zone). The insets show the simulated intensity distributions corresponding to these three distinct regimes, as obtained from Eqs. (3). Panel (d) presents the complex Berry phase Φ_- as a function of the normalized gain coefficient η.

towards the edge mode. Finally, for even higher values of gain or loss contrast, i.e., $\eta > \nu + 1$, the array crosses another threshold and moves into phase III, as also corroborated by analyzing Eqs. (3). At this point, all of the bulk modes of the active lattice break their $\mathcal{PT}$ symmetry, and as such, they start to lase—all competing for the gain. Unlike what happens in the first two phases, after crossing into phase III, the edge state is now obscured by bulk modes. This in turn results in a more uniform intensity profile, as shown in the inset in Fig. 4(c). In other words, in this range, the pumped sublattice is uniformly lasing, while its lossy counterpart remains dark. This can be explained by the fact that the carrier-induced detuning between adjacent resonators, which is by nature a nonlinear effect, significantly suppresses the coupling between neighboring units. The theoretically expected spectra corresponding to these three phases can be found in Ref. [33]. Our simulations also suggest that the boundary between phases I and II can be nonlinearly modified because of the linewidth enhancement factor α_H, something that is also revealed in our experiments. Moreover, because of nonlinear α_H-induced index changes, the lasing frequencies associated with the modes of this SSH system will be shifted with respect to that of a cold cavity. However, as indicated by the theoretically predicted spectra [33], this lasing frequency shift is expected to be considerably higher for bulk modes as opposed to that of a lasing edge state. This behavior can be explained by the fact that the nonlinear shift in frequency is essentially determined by the lasing threshold associated with a specific eigenstate [Eqs. (3)]. This is consistent with the fact that the $\mathcal{PT}$-symmetry breaking threshold for the lasing edge state is lower than that of bulk modes.

Interestingly, the onset of these three phases is also manifested in the complex Berry phase associated with this SSH laser array [33,36]. Figure 4(d) shows the Berry phase associated with the lower band Φ_- as a function of the normalized gain η when $\nu = 2$. This figure reveals that the geometric phase undergoes phase transitions at exactly the same boundaries ($\nu \pm 1$), as also previously indicated by Eq. (6). Note that the global Berry phase [36], defined as the sum of Φ_+ and Φ_- associated with the upper and lower bands, is independent of the gain and is nonzero in all the three phases (see Sec. 4 of Ref. [33]).

To verify these predictions, we conducted a series of experiments with a 16 microring resonator SSH array, each having a radius of 5 μm. To enforce single-transverse mode operation at 1.59 μm, the width of the resonators was set to 500 nm. In order to reduce the lasing threshold, the microrings were surrounded by a low-index dielectric, entailing a higher confinement. As previously indicated, each ring was individually interrogated (intensitywise and spectrally) through an extraction bus waveguide, featuring a pair of grating outcouplers [Fig. 1(c)]. To introduce $\mathcal{PT}$ symmetry, the microresonators were alternately pumped at 1.06 μm by using a titanium amplitude mask. Figure 5 shows the measured ring intensity and spectra using an InGaAs camera. In particular, Figs. 5(a), 5(b), and 5(c) present the data corresponding to phase I, II, and III, respectively. At a pump intensity of $I = 26$ kW/cm^2, only the edge mode lases [Fig. 5(a)]. Once the first phase transition occurs, other modes start competing for the gain [Fig. 5(b) at $I = 41$ kW/cm^2], and eventually the edge

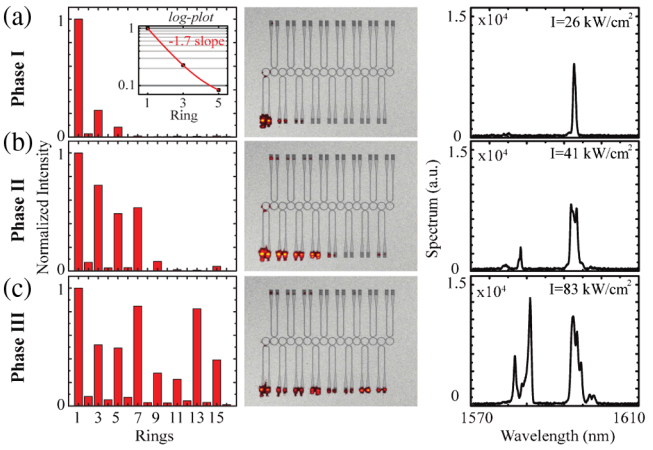

FIG. 5. The left panels depict the measured intensity distributions in the 16-element SSH array at every site. The middle panels show raw data from the extraction ports, while the right panels the corresponding power spectra. Each of the successive rows (a), (b), and (c) are progressively associated with phase I, II, and III observations. The inset in (a) provides the exponential intensity distribution of the lasing edge state in a log-linear scale.

mode is obscured [Fig. 5(c) at $I = 83$ kW/cm^2]. The emergence of these three phases is also evident in their spectra. While the spectrum of the edge mode is single moded, once the first phase transition occurs, bulk modes also appear, with shifted frequencies as expected from the theory [33]. Figure 5(a) indicates that the exponential intensity decay of the edge mode (log-linear inset) is in good agreement with the theory [$\propto (\kappa_1/\kappa_2)^{2n}$] when $\nu = 1.7$. In all our experiments, we found that gain saturation plays a prominent role in stabilizing the lasing edge mode at different pumping levels. Moreover, the same effects tend to shift the frequency of the bulk modes as a function of the pump power. Yet, the central frequency of the edge mode experiences a negligible shift, thus manifesting its robustness (see Sec. 1 of Ref. [33]).

In conclusion, we have observed for the first time lasing topological edge modes in an active SSH microring array. Under chiral-time symmetry, the transitions of this $\mathcal{PT}$-symmetric non-Hermitian system can be described through both the complex band structure and the corresponding complex Berry phase. The effects of gain saturation and carrier dynamics on the edge mode were also systematically investigated.

The authors gratefully acknowledge the financial support from Office of Naval Research (ONR) (N00014-16-1-2640), National Science Foundation (NSF) (ECCS-1454531, DMR-1420620, and ECCS-1757025), Air force Office of Scientific Research (AFOSR) (FA9550-14-1-0037), Binational Science Foundation (BSF) (2016381), and Army Research Office (ARO) (W911NF-16-1-0013 and W911NF-17-1-0481). This work was also partially funded by the Qatar National Research Fund (NPRP 9-020-1-006). This work was supported by European Commission Non-Hermitian Quantum Wave Engineering (NHQWAVE) project (MSCA-RISE 691209).

Note added in proof.—Before closing, we would like to note that recently two other similar works appeared in the literature [37].

*demetri@creol.ucf.edu
†mercedeh@creol.ucf.edu

[1] D. J. Thouless, M. Kohmoto, M. P. Nightingale, and M. den Nijs, Phys. Rev. Lett. **49**, 405 (1982).
[2] M. Z. Hasan and C. L. Kane, Rev. Mod. Phys. **82**, 3045 (2010).
[3] C. L. Kane and E. J. Mele, Phys. Rev. Lett. **95**, 226801 (2005).
[4] X.-L. Qi and S.-C. Zhang, Rev. Mod. Phys. **83**, 1057 (2011).
[5] F. D. M. Haldane and S. Raghu, Phys. Rev. Lett. **100**, 013904 (2008).
[6] Z. Wang, Y. Chong, J. D. Joannopoulos, and M. Soljacic, Nature (London) **461**, 772 (2009).
[7] C. Poli, M. Bellec, U. Kuhl, F. Mortessagne, and H. Schomerus, Nat. Commun. **6**, 6710 (2015).
[8] L. Lu, J. D. Joannopoulos, and M. Soljacic, Nat. Photonics **8**, 821 (2014).
[9] M. Hafezi, E. A. Demler, M. D. Lukin, and J. M. Taylor, Nat. Phys. **7**, 907 (2011).
[10] A. B. Khanikaev, S. H. Mousavi, W. K. Tse, M. Kargarian, A. H. MacDonald, and G. Shvets, Nat. Mater. **12**, 233 (2013).
[11] M. Hafezi, S. Mittal, J. Fan, A. Migdall, and J. M. Taylor, Nat. Photonics **7**, 1001 (2013).
[12] M. C. Rechtsman, J. M. Zeuner, Y. Plotnik, Y. Lumer, D. Podolsky, F. Dreisow, S. Nolte, M. Segev, and A. Szameit, Nature (London) **496**, 196 (2013).
[13] A. Blanco-Redondo, I. Andonegui, M. J. Collins, G. Harari, Y. Lumer, M. C. Rechtsman, B. J. Eggleton, and M. Segev, Phys. Rev. Lett. **116**, 163901 (2016).
[14] L. Tarruell, D. Greif, T. Uehlinger, G. Jotzu, and T. Esslinger, Nature (London) **483**, 302 (2012).
[15] M. Atala, M. Aidelsburger, J. T. Barreiro, D. Abanin, T. Kitagawa, E. Demler, and I. Bloch, Nat. Phys. **9**, 795 (2013).
[16] C. L. Kane and T. C. Lubensky, Nat. Phys. **10**, 39 (2014).
[17] Z. Yang, F. Gao, X. Shi, X. Lin, Z. Gao, Y. Chong, and B. Zhang, Phys. Rev. Lett. **114**, 114301 (2015).
[18] S. Malzard, C. Poli, and H. Schomerus, Phys. Rev. Lett. **115**, 200402 (2015).
[19] C. E. Bardyn, M. A. Baranov, C. V. Kraus, E. Rico, A. Imamoglu, P. Zoller, and S. Diehl, New J. Phys. **15**, 085001 (2013).
[20] D. Leykam, K. Y. Bliokh, C. Huang, Y. D. Chong, and F. Nori, Phys. Rev. Lett. **118**, 040401 (2017).
[21] H. Schomerus, Opt. Lett. **38**, 1912 (2013).
[22] C. E. Ruter, K. G. Makris, R. El-Ganainy, D. N. Christodoulides, M. Segev, and D. Kip, Nat. Phys. **6**, 192 (2010).
[23] H. Hodaei, M. A. Miri, M. Heinrich, D. N. Christodoulides, and M. Khajavikhan, Science **346**, 975 (2014).
[24] Y. Lumer, Y. Plotnik, M. C. Rechtsman, and M. Segev, Phys. Rev. Lett. **111**, 243905 (2013).
[25] H. Shen, B. Zhen, and L. Fu, arXiv:1706.07435.
[26] T. E. Lee, Phys. Rev. Lett. **116**, 133903 (2016).
[27] W. P. Su, J. R. Schrieffer, and A. J. Heeger, Phys. Rev. Lett. **42**, 1698 (1979).
[28] M. S. Rudner and L. S. Levitov, Phys. Rev. Lett. **102**, 065703 (2009).
[29] J. M. Zeuner, M. C. Rechtsman, Y. Plotnik, Y. Lumer, S. Nolte, M. S. Rudner, M. Segev, and A. Szameit, Phys. Rev. Lett. **115**, 040402 (2015).
[30] S. Weimann, M. Kremer, Y. Plotnik, Y. Lumer, S. Nolte, K. G. Makris, M. Segev, M. C. Rechtsman, and A. Szameit, Nat. Mater. **16**, 433 (2017).
[31] G. P. Agrawal and N. K. Dutta, *Semiconductor Lasers* (Springer, New York, 1993).
[32] A. U. Hassan, H. Hodaei, M. A. Miri, M. Khajavikhan, and D. N. Christodoulides, Phys. Rev. A **92**, 063807 (2015).
[33] See Supplemental Material at http://link.aps.org/supplemental/10.1103/PhysRevLett.120.113901 for theoretically predicted spectra emitted by the PT-symmetric

SSH laser array which includes Refs. [34,35]. The reason behind the frequency upshift associated with the lasing bulk modes is provided. The analytic field distributions for the topological edge states in the SSH array considered are also given, and the analytical form for the complex Berry phase associated with the Hamiltonian discussed here is presented.

[34] J. Garrison and E. Wright, Phys. Lett. A **128**, 177 (1988).

[35] J. Zak, Phys. Rev. Lett. **62**, 2747 (1989).

[36] S. D. Liang and G. Y. Huang, Phys. Rev. A **87**, 012118 (2013).

[37] P. St-Jean, V. Goblot, E. Galopin, A. Lemaître, T. Ozawa, L. Le Gratiet, I. Sagnes, J. Bloch, and A. Amo, Nat. Photonics **11**, 651 (2017); H. Zhao, P. Miao, M. H. Teimourpour, S. Malzard, R. El-Ganainy, H. Schomerus, and L. Feng, arXiv: 1709.02747.